Revision #2

In-situ infrared spectra of hydroxyl in wadsleyite and ringwoodite at high pressure and high temperature

XIAOZHI YANG[1,2], HANS KEPPLER[2], LEONID DUBROVINSKY[2] AND ALEXANDER KURNOSOV[2]

1. State Key Laboratory for Mineral Deposits Research, School of Earth Sciences and Engineering, Nanjing University, Nanjing 210046, PR China
2. Bayerisches Geoinstitut, Universität Bayreuth, D-95440 Bayreuth, Germany

ABSTRACT

The infrared spectra of hydroxyl in synthetic hydrous wadsleyite (β-Mg_2SiO_4) and ringwoodite (γ-Mg_2SiO_4) were measured at room temperature up to ~18.8 GPa for wadsleyite and up to ~21.5 GPa for ringwoodite. High-temperature spectra were measured in an externally heated diamond anvil cell up to 650 °C at ~14.2 GPa for wadsleyite and up to 900 °C at ~18.4 GPa for ringwoodite. The synthetic samples reproduce nearly all the important OH bands previously observed at ambient conditions. Only subtle changes were observed in the infrared spectra of both minerals, both upon compression at room temperature and upon heating at high pressure, For wadsleyite, upon compression to ~18.8 GPa, the frequencies of the bands at ~3600 cm^{-1} remain almost unchanged, while the main bands at 3200-3400 cm^{-1} shift to lower frequencies. During heating at 14.2 GPa to 650 °C the bands at 3200-3400 cm^{-1} broaden and shift to slightly lower frequencies. For ringwoodite, upon compression to ~21.5 GPa, the main bands at ~3115 cm^{-1} progressively shift to lower frequencies. During heating at 18.4 GPa to 900 °C, no frequency shift was observed for the band at ~3700 cm^{-1}, but the band initially at ~3115 cm^{-1} shifts very slightly to higher frequencies, which should yield almost the same band positions at ~1300-1400 °C as those measured at ambient conditions. Our data suggest that water speciation in hydrous wadsleyite and ringwoodite at ambient conditions may be

comparable to that under mantle conditions, except perhaps for subtle changes in hydrogen bonding. The low OH-stretching frequencies in wadsleyite and ringwoodite under transition zone conditions imply a large H/D fractionation during degassing of the deep mantle. This may explain the apparent disequilibrium between the hydrogen isotopic composition of the upper mantle and the ocean.

KEY WORDS

Hydroxyl, wadsleyite, ringwoodite, infrared spectra, high-pressure & high-temperature, diamond anvil cell

INTRODUCTION

Wadsleyite (β-Mg_2SiO_4) and ringwoodite (γ-Mg_2SiO_4), the high pressure polymorphs of olivine (α-Mg_2SiO_4), are the most abundant minerals in the transition zone of Earth's mantle, between 410- and 660-km depth. Both minerals are able to accommodate up to several percent (by weight) of water as hydroxyl groups in their structure, and they likely constitute the most important water reservoir in Earth's interior (e.g. Smyth 1987; Kohlstedt et al. 1996; Bolfan-Casanova et al. 2000). Water strongly affects many physical and chemical properties of wadsleyite and ringwoodite, including elastic moduli, seismic velocities, molar volume, rheological strength, thermal expansion, and electrical conductivity (Inoue et al. 1998; Kavner 2003; Smyth et al. 2003; Inoue et al. 2004; Jacobsen et al. 2004; Huang et al. 2005; Ye et al. 2009). The water contents in wadsleyite and ringwoodite can be high enough to shift phase boundaries between solid phases and to drastically reduce melting temperatures. As such, they may affect the structure of the transition zone, in particular the depth and width of the 410-km discontinuity and they may influence convection and dynamics of the whole mantle (Wood 1995; Bercovici and Karato 2003; Frost and Dolejs 2007; Richard and Bercovici 2009; Deon et al., 2013).

Structural models of the incorporation of H into wadsleyite and ringwoodite are indispensable for understanding water storage in the mantle and for predicting the effect of hydrogen on physical and chemical properties of the transition zone. Infrared spectroscopy is particularly useful for revealing the speciation of H in

minerals, and so far models of the dissolution of H in wadsleyite and ringwoodite have been derived mostly from infrared spectra (e.g. Bolfan-Casanova et al. 2000; Jacobsen et al. 2005; Deon et al., 2010; Panero et al. 2013). Neutron diffraction (Sano-Furukawa et al. 2011) and NMR studies (Stebbins et al. 2009; Griffin et al. 2013) have generally confirmed the structural models derived from infrared spectroscopy, although they have added a number of important details. Water dissolution in wadsleyite is generally well understood. The wadsleyite structure contains an Si_2O_7 group and one oxygen atom (O1) not attached to silicon. Smyth (1987) pointed out that this oxygen atom is electrostatically underbonded and should be a suitable site for protonation. In hydrous wadsleyite, protonation of O1 is charge compensated by Mg^{2+} vacancies. The intense bands between 3300 and 3400 cm^{-1} in the infrared spectrum of hydrous wadsleyite can be assigned to this substitution mechanism, with the OH vector pointing from the O1 atom to the O4 atom along a vacant M3 octahedral site. The weaker bands at ~3600 cm^{-1} may be due to bent hydrogen bonds along the M3 edge, and the bands at ~3000 cm^{-1} may be assigned to protonation of the tetrahedral edge of the Si_2O_7 group (Smyth 1987; Bolfan-Casanova et al. 2000; Jacobsen et al. 2005; Deon et al. 2010; Sano-Furukawa et al. 2011; Griffin et al. 2013). The high water solubility in ringwoodite is more difficult to understand, as ringwoodite has a spinel structure and spinels usually do not dissolve any measurable amount of water. The dissolution of water is probably mostly related to Mg^{2+} vacancies on the octahedral sites, but substitution of Mg^{2+} for Si^{4+} on the tetrahedral site and perhaps silicon vacancies with a hydrogarnet type

defect may also be involved (Kudoh et al. 2000; Smyth et al. 2003; Mrosko et al., 2013). The infrared spectra of hydrous ringwoodite show a very broad band at ~3115 cm^{-1} and some smaller bands at ~3695 and 2500 cm^{-1}. Possibly, the band at ~3695 cm^{-1}, which only appears at high water contents, is related to partial protonation of the octahedral edges, the band at 3115 cm^{-1} is due to protonation on the edges of the tetrahedral sites, and the bands at 2500 cm^{-1} are overtones of the in-plane X-OH bending modes or their combination with other vibrations (Bolfan-Casanova et al. 2000; Smyth et al. 2003; Chamorro Pérez et al. 2006). However, a number of other assignments of these bands have also been suggested; these include the assignment of the 3695 cm^{-1} band to a hydrogarnet-type defect of four protons substituting for a Si vacancy (Blanchard et al. 2009; Mrosko et al. 2013) and the suggestion that the broad OH band at 3115 cm^{-1} corresponds to the protonation of octahedral edges (Kudoh et al 2000; Blanchard et al. 2009). This uncertainty in the band assignment is mostly due to the cubic symmetry of ringwoodite, which precludes the observation of infrared pleochroism. Recent studies, based on annealing experiments (Mrosko et al. 2013) and low-temperature FTIR (Panero et al. 2013), suggest that the broad main band of ringwoodite at 3115 cm^{-1} actually consists of several sub-bands involving different proton locations.

Up to now, models of hydrogen dissolution in wadsleyite and ringwoodite have been based exclusively on spectroscopic and diffraction data obtained at room temperature. Therefore, it is uncertain whether the available models correctly

104 describe the hydrogen substitution mechanisms deep in the mantle. Given the high
105 mobility of H, it is quite possible that its location may change upon quenching of a
106 sample from high temperature and pressure. In particular, the very broad main band
107 of ringwoodite could be due to some proton disordering during quenching. In order
108 to provide additional insights into the true hydrogen speciation in wadsleyite and
109 ringwoodite at mantle conditions, we present here in-situ FTIR spectra of hydrous
110 wadsleyite and ringwoodite at simultaneous high-pressure and high-temperature
111 conditions.
112
113 **EXPERIMENTAL METHODS**
114 The starting material for the synthesis of hydrous Mg_2SiO_4 wadsleyite and
115 ringwoodite were two high-purity synthetic single crystals of forsterite (diameter, 1.0
116 mm; length, 1.0 mm). A mixture of talc plus brucite powder with a weight ratio of
117 1.4:1 was added as water source (corresponding to several percent H_2O relative to
118 the entire charge). For each experiment, the starting materials were sealed in a
119 welded Pt capsule (outer diameter, 1.6 mm; inner diameter, 1.3 mm; length, ~3 mm).
120 The syntheses were carried out in a 1200-tonne multi anvil apparatus at 18 GPa and
121 1400 °C for wadsleyite and at 22 GPa and 1400 °C for ringwoodite, using a 10/5 and
122 10/4 octahedral assembly (octahedron length/truncation length) and a lanthanum
123 chromate heater. The run duration was 200 min. Temperature was monitored and
124 controlled to within ±1 °C during the experiments using a W3%Re/W25%Re
125 thermocouple. At the end of the experiment, the sample was quenched to room

126 temperature within several seconds by switching off the power to the heating circuit.
127 The recovered crystals were of high quality, free of any visible impurities or
128 inclusions and up to ~300 μm in size. Water contents of the synthesized samples
129 were determined by unpolarized infrared analysis on doubly-polished thin sections
130 (~30 μm thick) at ambient conditions. The spectra were integrated from 2300 to
131 3800 cm^{-1} and water contents were determined using the mineral-specific extinction
132 coefficients of 73000 L/(mol·cm^2) for wadsleyite by Deon et al. (2010) and of
133 100000 L/(mol·cm^2) for ringwoodite by Koch-Müller and Rhede (2010). The
134 estimated water content is ~1.5% H_2O for the wadsleyite and ~1.1% H_2O for the
135 ringwoodite.
136
137 Hydrostatic high-pressure and high-temperature conditions were generated in a
138 symmetric piston-cylinder-type diamond anvil cell (DAC) with diamonds of 300 μm
139 culet size and an external resistive heater. Prior to sample loading, a piece of Re foil
140 (~200 μm thickness and ~0.4 × 0.4 cm length × width) was pre-indented in the cell
141 to a thickness of ~40 μm. A 150-μm-diameter hole was then drilled into the gasket. A
142 ~15 μm thick thin section of the sample, with length and width of about 40 and 50
143 μm, was loaded into the sample chamber between two diamond anvils together with
144 a <8-μm-diameter ruby sphere for pressure calibration. The sample chamber was
145 then filled with Ne gas as pressure transmitting medium at ~0.15 GPa using a
146 high-pressure gas-loading apparatus developed at the Bayerisches Geoinstitut. The
147 cell was sealed at 1-2 GPa. Two loadings were prepared for each mineral: one for

compression to high pressure at room temperature and the other one for heating to high temperature at constant pressure (~14.2 GPa for wadsleyite and ~18.4 GPa for ringwoodite). In the high temperature runs, the resistive heater was placed inside the DAC and around the gasket between the diamond anvils (in air), and an S-type thermocouple (Pt-$Pt_{90}Rh_{10}$), located very close to the gasket hole (~200 μm distance), was used to estimate temperature. The pressure prior to and after each infrared analysis was determined by ruby fluorescene with a Jobin Yvon Labram spectrometer as calibrated for hydrostatic conditions by Mao et al. (1986) and Rekhi et al. (1999). For each measurement, the variation of pressure was <0.2 GPa, usually <0.1 GPa, and the variation of temperature was <1 °C as recorded by the S-type thermocouple.

For the experiments at room temperature, infrared spectra were recorded using a Bruker IFS 120 spectrometer coupled to a Bruker IR microscope (IR scope I); while for the experiments at high temperature, infrared spectra were obtained using a Bruker IFS 125 spectrometer with the same microscope. For each measurement, 70 to 200 scans were acquired with 4 cm^{-1} resolution using a tungsten light source, a Si-coated CaF_2 beam splitter and a narrow-band MCT detector. During the measurements, the spectrometer was evacuated and the optics of the microscope was continuously purged with H_2O- and CO_2-free, purified air. The background spectra were measured through the diamonds inside the Ne-filled gasket holes. The band positions of each spectrum were obtained by deconvoluting the spectra into Gaussian

components using the Peakfit program (Ver. 4.12, Systat Software Inc.). Interference fringes in the spectra, due to multiple reflections between a sample and diamond surfaces, were removed either by the method developed by Neri et al. (1987) or were deconvoluted with the Peakfit software together with the OH bands of the sample. Recovered samples were examined by Raman spectroscopy; no irreversible phase changes were found.

RESULTS AND DISCUSSION

Spectra at ambient conditions

Infrared spectra of the synthesized hydrous wadsleyite and ringwoodite collected at ambient conditions, at high pressures (room temperature) and at high temperatures (with pressure maintained at ~14.2 GPa for wadsleyite and ~18.4 GPa for ringwoodite) are illustrated in Fig. 1 and 2, together with spectra of the samples at ambient conditions after the experiments. At ambient conditions, the samples show the typical OH-related absorption bands in the 2300-3800 cm^{-1} range previously reported for the corresponding mineral. For wadsleyite, the spectrum shows bands at ~3660, 3582, 3360 and 3320 cm^{-1}, similar to those reported by Bolfan-Casanova et al. (2000), Jacobsen et al. (2005) and Deon et al. (2010), but the weak absorption centered at ~3000 cm^{-1} observed in some studies is not obvious in our sample (Fig. 1a). For ringwoodite, the spectrum contains a broad and strong band at ~3115 cm^{-1}, a weaker band at ~3695 cm^{-1}, and one weak doublet at ~2500 cm^{-1} (with two bands at ~2550 and 2472 cm^{-1}, respectively). Similar to observations in previous studies

(Bolfan-Casanova et al. 2000; Smyth et al. 2003; Chamorro Pérez et al. 2006). For both wadsleyite and ringwoodite, the spectra prior to and after either compression (Fig. 1a and 2a) or heating (Fig. 1b and 2b) show no distinctive differences, and the band frequencies of the samples are reversible upon decompression (Fig. 3a and 4a) or cooling (Fig. 3b and 4b), implying the absence of phase transitions, system hysteresis and H diffusion loss during the runs.

Behavior of wadsleyite upon compression and heating

Upon compression of wadsleyite to ~18.8 GPa (Fig. 1a and 3a), the two bands at ~3660 and 3582 cm^{-1} remain almost unchanged, while the bands at 3360 and 3320 cm^{-1} progressively shift to lower frequencies. The general trends of the band positions with increasing pressure are similar to those previously observed by Raman spectroscopy (Kleppe et al., 2001) and by FTIR (Deon et al., 2010) for hydrous wadsleyite (β-Mg_2SiO_4) with different water contents (~1.6% H_2O in the former and 0.8% H_2O in the latter study). The frequency shift for the bands initially at 3360 and 3320 cm^{-1} is best described by by second-order polynomial fits with first and second order pressure derivatives of -9.80 cm^{-1}/GPa and 0.13 cm^{-2}/GPa^2 for the band at 3360 cm^{-1} and of -10.18 cm^{-1}/GPa and 0.09 cm^{-1}/GPa^2 for the band at 3320 cm^{-1}. The difference to the linear fits given by Kleppe et al. (2001) and Deon et al. (2010) may be due to a different deconvolution of the bands. For example, in Deon et al. (2010), the main broad band was resolved into three components in contrast to the two bands in the present study; while in Kleppe et al. (2001), the resolution of

the Raman spectra was not sufficient for further deconvolution.

High-temperature spectra of wadsleyite at 14.2 GPa up to 650 °C are shown in Figure 1b. The positions of the two bands at ~3660 and 3582 cm^{-1} do not seem to change much, although the appearance of relatively strong interference fringes in the spectra makes it difficult to precisely locate these bands. Not that the intensity of these interference fringes is very sensitive to the degree of parallelity of sample surfaces and to the beam path through the diamond cell, so that major changes may occur for different experiments, even for samples from the same charge. The bands initially at 3320 cm^{-1} and at 3360 cm^{-1} at ambient conditions cannot be well resolved from each other anymore, but the envelope of the two bands appears to shift slightly to lower frequencies with the temperature derivative of 0.03 cm^{-1}/°C (Fig. 3b).

Behavior of ringwoodite upon compression and heating

High-pressure spectra of ringwoodite are shown in Figure 2a. Unfortunately, the occurrence of interference fringes makes it difficult to locate the weaker bands, but the main band at 3115 cm^{-1} gradually shifts to lower frequencies. A similar behavior of hydrous ringwoodite under pressure was observed by Chamorro Pérez et al. (2006) and by Koch-Müller et al. (2011). The shift of the band initially at ~3115 cm^{-1} may be described by a second order polynomial fit, which gives first and second order pressure derivatives of -12.3 cm^{-1}/GPa and 0.23 cm^{-1}/GPa^2, agreeing well with the reported -12.1 cm^{-1}/GPa and 0.20 cm^{-1}/GPa^2 by Chamorro Pérez et al. (2006).

Upon heating the ringwoodite to 900 °C at ~18.4 GPa, no frequency shift was observed for the band at ~3695 cm^{-1}, but the band at ~2970 cm^{-1}, initially at ~3115 cm^{-1} at ambient conditions, shifts very slowly to higher frequencies (Fig. 2b and 4b). The band initially located at ~2970 cm^{-1} can be best fitted by a linear function, with the temperature derivative of 0.10 cm^{-1}/°C. A closer inspection of the spectra reveals that at 18.4 GPa and 27 °C, a shoulder is visible at the high-frequency side of the main absorption peak. Deconvolution of the spectra suggests that this shoulder is due to a Gaussian component at ~3367 cm^{-1}. This agrees well with a separate component in the ringwoodite spectrum detected by low-temperature FTIR spectroscopy (Panero et al. 2013). At higher temperatures, this shoulder becomes less prominent; however, deconvolution of the spectrum measured at 900 °C suggests that it is still present, although perhaps with somewhat reduced intensity (Fig. 5).

Implications for water storage in the transition zone

Temperatures in the transition zone of Earth´s mantle, where wadsleyite and ringwoodite are stable, are expected to be in the range of 1400 to 1600 °C (Ito and Katsura 1989). Unfortunately, with present technology it is not possible to do infrared spectroscopy in-situ under these conditions; the 900 °C reached in our measurements with ringwoodite are already close to the upper temperature limit of externally heated diamond anvil cells. Directly probing the speciation of hydrogen in minerals under transition zone conditions would likely require the use of a different technology, such as high-pressure neutron diffraction. However, the data presented

here are at least consistent with the hypothesis that water speciation in wadsleyite and ringwoodite under transition zone conditions is not fundamentally different from that inferred from studies at ambient conditions.

A particularly important result of our study is that the strength of hydrogen bonding in wadsleyite and ringwoodite under transition zone conditions may be similar to that under ambient conditions. In particular for ringwoodite, the effects of increasing pressure and increasing temperature on the OH stretching frequency nearly cancel out. It has been shown by Dobson et al. (1989) that, based on the measured H/D fractionation factors of 12 minerals (pectolite, diaspore, zoisite, boehmite, epidote, muscovite, kaolinite, biotite, hornblende, annite, phlopopite and chrysotile) and of two glasses (rhyolitic obsidian and albite-orthoclase glass), a very good negative correlation exists between the OH stretching frequency in a mineral and the H/D isotopic fractionation factor between the mineral and water vapor (Fig. 6). Such a correlation of hydrogen bond strength with the fractionation factor is theoretically expected, and has been partly confirmed for mantle samples by Bell and Ihinger (2000). They observed that nominally anhydrous mantle augite, orthopyroxene and garnet, characterized by lower OH stretching frequency (3560-3460 cm^{-1}) relative to phlogopite (3660-3710 cm^{-1}), generally have lower δD (-90‰ to -110‰) than phlogopite (typically δD = -80‰,). Moreover, the results of Dobson et al. (1989) demonstrate that the H/D fractionation curves as a function of temperature are usually parallel between different minerals, indicating that the relative fractionation

between the mineral pairs would be much less affected by temperature than the fractionation between the minerals and water vapor. The stretching frequencies in wadsleyite and particularly in ringwoodite are very low compared to most other hydrous minerals, such as serpentine, amphibole and micas. This would imply that H/D fractionation between wadsleyite and particularly ringwoodite and water vapor should be much stronger than for the minerals formed by water-rock interaction on the ocean floor. For example, the predicted fractionation factor of ringwoodite is ~90‰ at 18.4 GPa and 400 °C (Fig. 6). Possibly, this could provide an explanation for the large difference in hydrogen isotopic composition between seawater (δD = 0‰) and the upper mantle (δD = -80‰), which is difficult to explain by equilibrium between these two reservoirs (Shaw et al. 2008 and references therein). As wadsleyite and ringwoodite are the main reservoirs of water in the mantle (e.g. Bolfan-Casanova et al. 2000) and as the oceans likely formed by degassing of Earth's interior, the isotopic composition of the ocean may reflect equilibrium isotope fractionation between a hydrous fluid and wadsleyite or ringwoodite. The low OH stretching frequency of these minerals would suggest that this process should lead to a strong depletion of deuterium in the solid residue. The present, strongly deuterium-depleted hydrogen isotope composition of the upper mantle may then be inherited from this initial transition zone signature by mantle mixing and upwelling.

ACKNOWLEDGEMENTS

We thank Hongzhan Fei for supplying the starting forsterite single crystal, Geeth Manthilake for technical assistance with multi-anvil experiments, Konstantin Glazyrin for help with gas loading, Hubert Schulze for sample preparation and Sven Linhardt for technical assistance with external heating. Comments from Monika Koch-Müller and one anonymous reviewer helped to improve the manuscript. This study was supported by the Alexander von Humboldt Foundation, the Bayerisches Geoinstitut visitors program and partly by the Recruitment Program of Global Young Experts (P.R. China).

REFERENCES CITED

Bell, D.R. and Ihinger, P.D. (2000) The isotopic composition of hydrogen in nominally anhydrous mantle minerals. Geochimica et Cosmochimica Acta, 64, 2109-2118.

Bercovici, D. and Karato, S. (2003) Whole-mantle convection and the transition-zone water filter. Nature, 425, 39-44.

Blanchard, M., Balan, E., and Wright, K. (2009) Incorporation of water in iron-free ringwoodite: a first-principles study. American Mineralogist, 94, 83-89.

Bolfan-Casanova, N., Keppler, H., and Rubie, D.C. (2000) Water partitioning between nominally anhydrous minerals in the MgO-SiO_2-H_2O system up to 24 GPa: implications for the distribution of water in the Earth's mantle. Earth and Planetary Science Letters, 182, 209-221.

Chamorro Pérez, E.M., Daniel, I., Chervin, J.-C., Dumas, P., Bass, J.D., and Inoue, T. (2006) Synchrotron IR study of hydrous ringwoodite (γ-Mg_2SiO_4) up to 30 GPa. Physics and Chemistry of Minerals, 33, 502-510.

Deon, F., Koch-Müller, M., Rhede, D., Gottschalk, M., Wirth, R., and Thomas, S.M. (2010) Location and quantification of hydroxyl in wadsleyite: new insights. American Mineralogist, 95, 312-322.

Deon, F., Koch-Müller, M., Rhede, D., and Wirth, R. (2013) Water and iron effect on the P-T-x coordinates of the 410-km discontinuity in the Earth upper mantle. Contributions to Mineralogy and Petrology, 161, 653-666.

Dobson, P.F., Epstein, S., and Stolper, E.M. (1989) Hydrogen isotope fractionation between coexisting vapor and silicate glasses and melts at low pressure. Geochimica et Cosmochimica Acta, 53, 2723-2730.

Frost, D.J. and Dolejs, D. (2007) Experimental determination of the effect of H_2O on the 410-km seismic discontinuity. Earth and Planetary Science Letters, 256, 182-195.

Griffin, J.M., Berry, A.J., Frost, D.J., Wimperis, S., and Ashbrook, S.E. (2013) Water in the Earth´s mantle: a solid-state NMR study of hydrous wadsleyite. Chemical Science, 4, 1523-1538.

Huang, X., Xu, Y., and Karato, S.I. (2005) Water content in the transition zone from electrical conductivity of wadsleyite and ringwoodite. Nature, 434, 746-749.

Inoue, T., Tanimoto, Y., Irifune, T., Suzuki, T., Fukui, H., and Ohtaka, O. (2004) Thermal expansion of wadsleyite, ringwoodite, hydrous wadsleyite and hydrous ringwoodite. Physics of the Earth and Planetary Interiors, 143-44, 279-290.

Inoue, T., Weidner, D.J., Northrup, P.A., and Parise, J.B. (1998) Elastic properties of hydrous ringwoodite (γ-phase) in Mg_2SiO_4. Earth and Planetary Science Letters, 160, 107-113.

Ito, E. and Katsura, T. (1989) A temperature profile of the mantle transition zone. Geophysical Research Letters, 16, 425-428.

Jacobsen, S.D., Demouchy, S., Frost, D.J., Ballaran, T.B., and Kung, J. (2005) A systematic study of OH in hydrous wadsleyite from polarized FTIR spectroscopy and single-crystal X-ray diffraction: Oxygen sites for hydrogen storage in Earth's interior. American Mineralogist, 90, 61-70.

Jacobsen, S.D., Smyth, J.R., Spetzler, H., Holl, C.M., and Frost, D.J. (2004) Sound velocities and elastic constants of iron-bearing hydrous ringwoodite. Physics of the Earth and Planetary Interiors, 143-144, 47-56.

Kavner, A. (2003) Elasticity and strength of hydrous ringwoodite at high pressure. Earth and Planetary Science Letters, 214, 645-654.

Kleppe, A.K., Jephcoat, A.P., Olijnyk, H., Slesinger, A.E., Kohn, S.C., and Wood, B.J. (2001) Raman

spectroscopic study of hydrous wadsleyite (β-Mg_2SiO_4) to 50 GPa. Physics and Chemistry of Minerals, 28, 232-241.

Koch-Müller, M. and Rhede, D. (2010) IR absorption coefficients for water in nominally anhydrous high-pressure minerals. American Mineralogist, 95, 770-775.

Koch-Müller, M., Speziale, S., Deon, F., Mrosko, M., and Schade, U. (2011) Stress-induced proton disorder in hydrous ringwoodite. Physics and Chemistry of Minerals, 38, 65-73.

Kohlstedt, D.L., Keppler, H., and Rubie, D.C. (1996) Solubility of water in the α, β, and γ phases of $(Mg,Fe)_2SiO_4$. Contributions to Mineralogy and Petrology, 123, 345-357.

Kudoh, Y., Kuribayashi, T., Mizobata, H., and Ohtani, E. (2000) Structure and cation disorder of hydrous ringwoodite, γ-$Mg_{1.89}Si_{0.98}H_{0.30}O_4$. Physics and Chemistry of Minerals, 27, 474-479.

Mao, H.K., Xu, J., and Bell, P.M. (1986) Calibration of the ruby presure gauge of 800 kbar under quasi-hydrostatic conditions. Journal of Geophysical Research, 91, 4673-4676.

Mrosko, M., Lenz, S., McCammon, C.A., Taran, M., Wirth, R., and Koch-Müller, M. (2013) Hydrogen incorporation and the oxidation state of iron in ringwoodite: A spectroscopic study. American Mineralogist, 98, 629-636.

Neri, F., Saitta, G., and Chiofalo, S. (1987) A simple procedure to remove the interference fringes from optical spectra. Journal of Physics E: Scientific Instruments, 20, 894-896.

Panero, W.R., Smyth, J.R., Pigott, J.S., Liu, Z., and Frost, D.J. (2013) Hydrous ringwoodite to 5 K and 35 GPa: Multiple hydrogen bonding sites resolved with FTIR spectroscopy. American Mineralogist, 98, 637-642.

Rekhi, S., Dubrovinsky, L.S., and Saxena, S.K. (1999) Temperature-induced ruby fluorescene shifts up to a pressure of 15 GPa in an externally heated diamond anvil cell. High Temperatures - High Pressures, 31, 299-305.

Richard, G.C. and Bercovici, D. (2009) Water-induced convection in the Earth´s mantle transition zone. Journal of Geophysical research, 114, B01205, doi: 10.1029/2008JB005734.

Sano-Furukawa, A, Kuribayashi, T., Komatsu, K., Yagi, T., and Ohtani, E. (2011) Investigation of hydrogen sites of wadsleyite: A neutron diffraction study. Physics of the Earth and Planetary Interiors, 198, 56-62.

Shaw, A.M., Hauri, E.H., Fischer, T.P., Hilton, D.R., Kelley, K.A. (2008) Hydrogen isotopes in Mariana arc melt inclusions: Implications for subduction dehydration and the deep-Earth water cycle. Earth and Planetary Science Letters, 275, 138-145.

Smyth, J.R. (1987) β-Mg_2SiO_4: a potential host for water in the mantle. American Mineralogist, 72, 1051-1055.

Smyth, J.R., Holl, C.M., Frost, D.J., Jacobsen, S.D., Langenhorst, F., and McCammon, C.A. (2003) Structural systematics of hydrous ringwoodite and water in Earth's interior. American Mineralogist, 88, 1402-1407.

Stebbins, J.F., Smyth, J.R., Panero, W.R., and Frost, D.J. (2009) Forsterite, hydrous and anhydrous wadsleyite and ringwoodite (Mg_2SiO_4): ^{29}Si NMR results for chemical shift anisotropy, spin-lattice relaxation, and mechanism of hydration. American Mineralogist, 94, 905-915.

Wood, B.J. (1995) The effect of H_2O on the 410-km depth discontinuity. Science, 268, 74-76.

Ye, Y., Schwering, R.A., and Smyth, J.R. (2009) Effect of hydration on thermal expansion of forsterite, wadsleyite and ringwoodite at ambient pressure. American Mineralogist, 94, 899-904.

Figure captions

Fig. 1 In situ infrared spectra of wadsleyite (a) to ~18.8 GPa at room temperature, and (b) to 650 °C at ~14.2 GPa. The spectra were normalized to 1 mm thickness and vertically offset. The spectrum in (a), labeled as after decompression, was measured from the sample after final decompression. The grey spectra in (b), labeled as 400, 200 and 25 °C, respectively, were measured during cooling, and the dashed spectrum in (b), labeled as Room-*P* & *T*, was measured at ambient conditions, as was the one labeled as 1 bar in (a). The variation of pressure before and after each measurement was usually less than 0.1 GPa for (a) and less than 0.2 GPa for (b). All the spectra were measured within the DAC.

Fig. 2 In situ infrared spectra of ringwoodite (a) to ~21.5 GPa at room temperature, and (b) to 900 °C at ~18.4 GPa. The spectra were normalized to 1 mm thickness and vertically offset. The spectrum in (a), labeled as after decompression, was measured from the sample after final decompression (note that the crystal cracked during the final rapid decompression). The grey spectra in (b), labeled as 200, 100 and 27 °C, respectively, were measured during cooling, and the dashed spectrum in (b), labeled as Room-*P* & *T*, was measured at ambient conditions, as was the one labeled as 1 bar in (a). The variation of pressure before and after each measurement was usually less than 0.1 GPa for (a) and less than 0.2 GPa for (b). All the spectra were measured within the DAC.

Fig. 3 Frequencies of OH bands in wadsleyite as a function of (a) pressure (room temperature), and (b) temperature (~14.2 GPa). Only the most prominent bands are

shown. The uncertainty in the frequencies is usually smaller than the symbol size. The curved lines are from second-order polynomial fits: in (a), band initially at ~3360 cm^{-1}, $\nu = 3361(\pm2) - 9.80(\pm0.68) \times P + 0.13(\pm0.03) \times P^2$, band initially at ~3320 cm^{-1}, $\nu = 3324(\pm2) - 10.18(\pm0.53) \times P + 0.09(\pm0.02) \times P^2$; in (b), band at ~3220 cm^{-1}, $\nu = 3223(\pm2) + 0.03(\pm0.01) \times T - 1.43\times10^{-4}$ $(\pm0.21\times10^{-4}) \times T^2$, where ν is frequency (cm^{-1}), P is pressure (GPa) and T is temperature (°C).

Fig. 4 Frequencies of OH bands in ringwoodite as a function of (a) pressure (room temperature), and (b) temperature (~18.4 GPa). Only the most prominent bands are shown. The uncertainty in the frequencies is usually smaller than the symbol size. For the band initially at ~3115 cm^{-1}, the curved line in (a) is from a second-order polynomial fit: $\nu = 3116(\pm2) - 12.3(\pm 0.6) \times P + 0.23(\pm 0.03) \times P^2$; and the line in (b) is from a linear fit: $\nu = 2952(\pm3) + 0.10 (\pm 0.01) \times T$, where ν is frequency (cm^{-1}), P is pressure (GPa) and T is temperature (°C).

Fig. 5. Deconvolution of the FTIR specta of ringwoodite at 18.4 GPa: (a) at 27 °C and (b) at 900 °C. The spectra were deconvoluted by the Peakfit software ($r^2 > 0.99$ for the fitting). The resolved shoulder component is ~3367 cm^{-1} at 27 °C (see text). The bands at ~2500 cm^{-1} cannot be reasonably resolved due to interference (Fig. 2b), and the added components here were only for fitting.

Fig. 6 Fractionation factor (1000 ln $\alpha_{vapor\text{-}mineral}$) of H between minerals and water vapor at 400 °C (modified after Dobson et al. (1989) and Bell and Ihinger (2000)). The average OH frequency of ringwoodite (vertical thick line) at 18.4 GPa and 400 °C is ~3000 cm^{-1} according to our results, yielding a fractionation factor of

440 ~90‰.

This is a preprint, the final version is subject to change, of the American Mineralogist (MSA)
Cite as Authors (Year) Title. American Mineralogist, in press.
(DOI will not work until issue is live.) DOI: http://dx.doi.org/10.2138/am.2014.4634

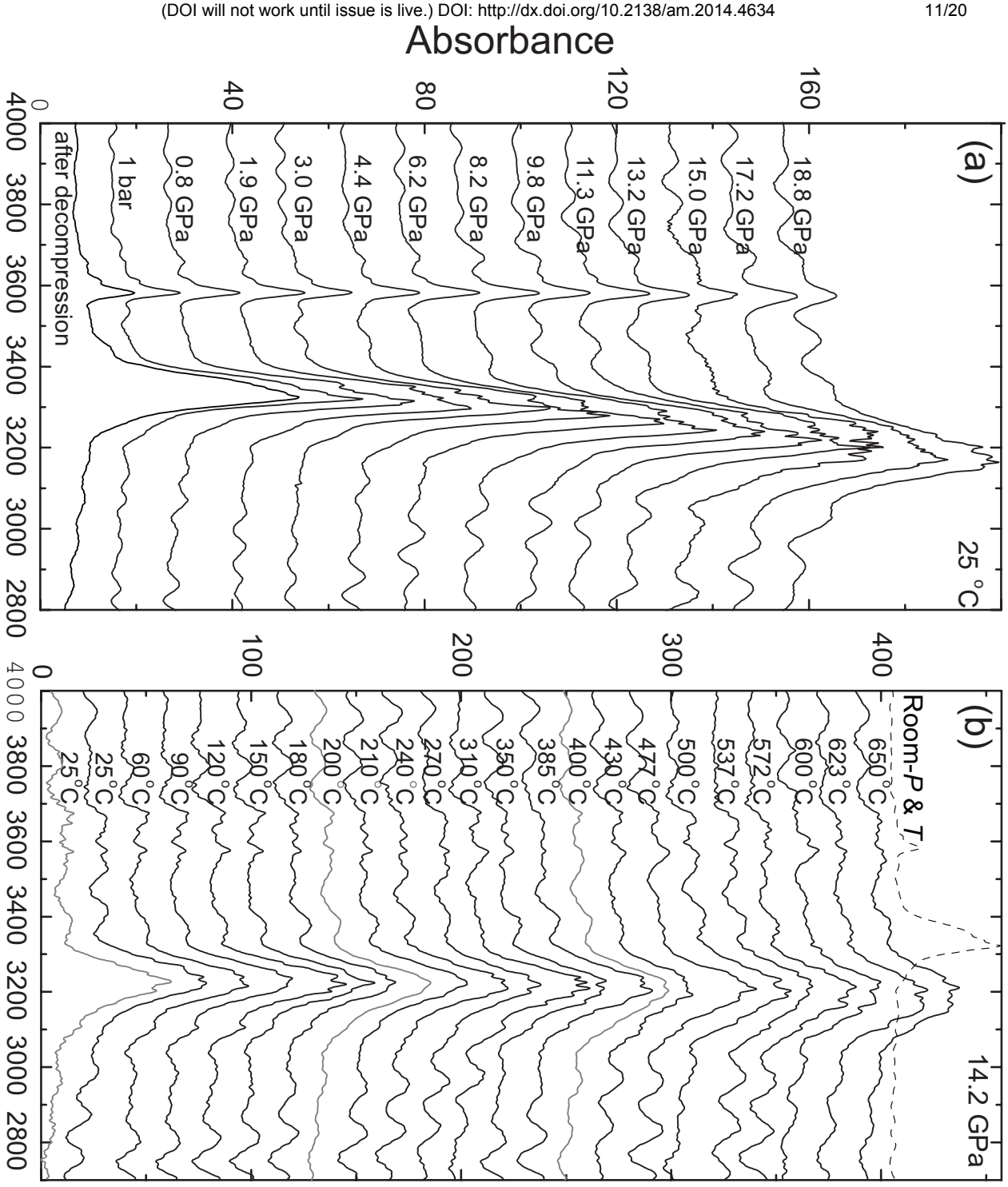

Fig.1

This is a preprint, the final version is subject to change, of the American Mineralogist (MSA)
Cite as Authors (Year) Title. American Mineralogist, in press.
(DOI will not work until issue is live.) DOI: http://dx.doi.org/10.2138/am.2014.4634

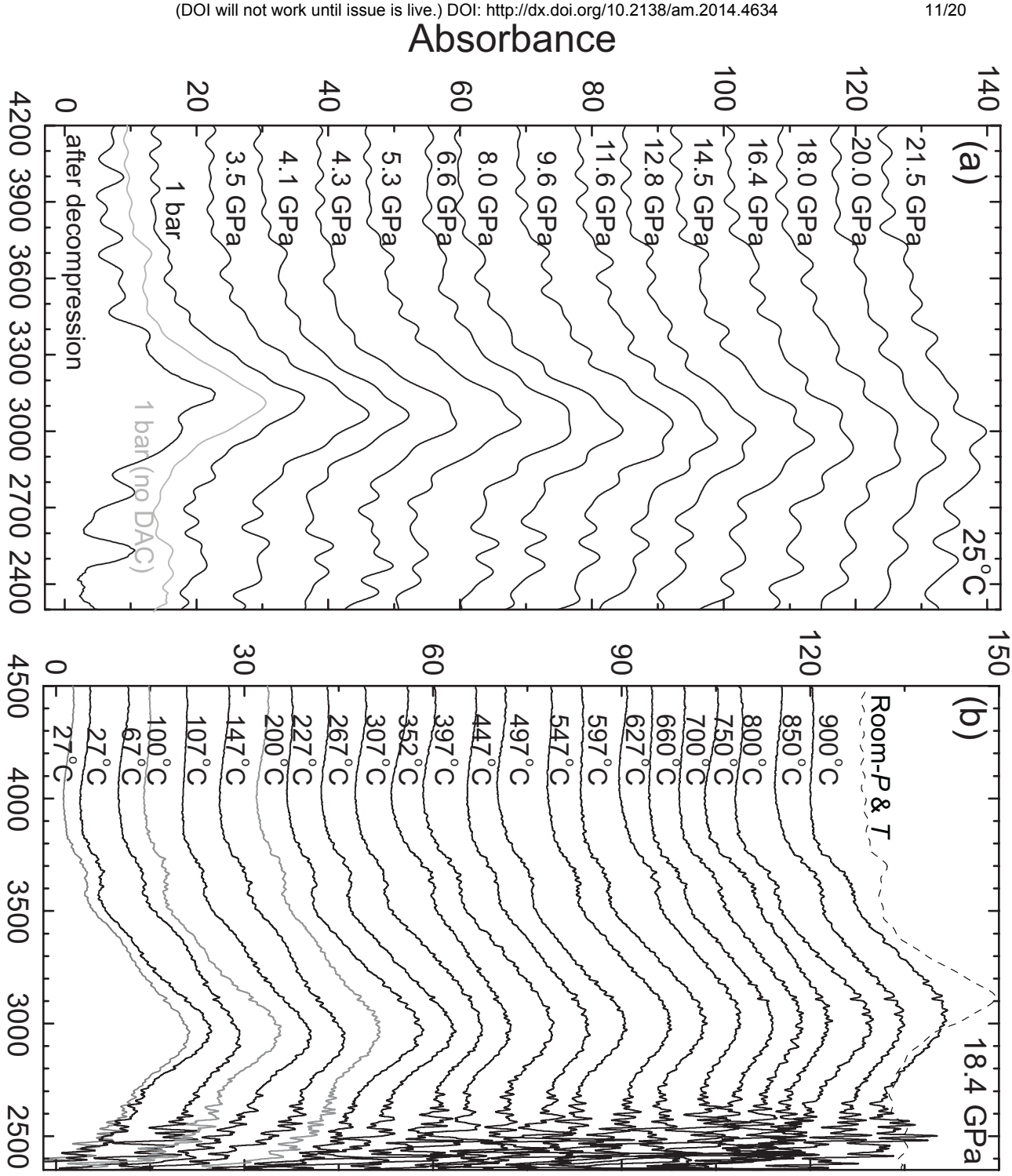

Fig.2

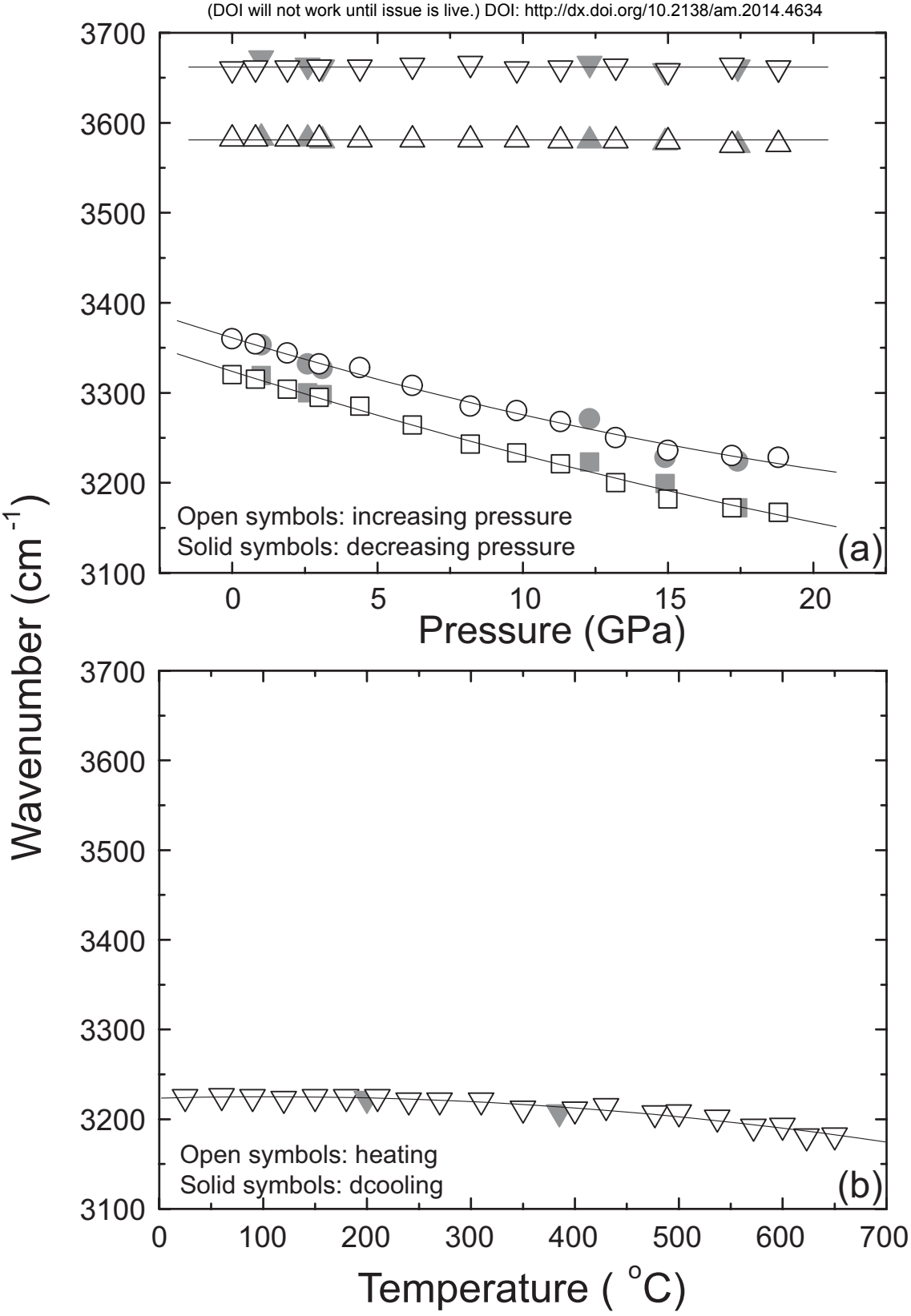
Wavenumber (cm^{-1})
3700
3600
3500
3400
3300
3200
3100
Open symbols: increasing pressure
Solid symbols: decreasing pressure
(a)
0
5
10
15
20
Pressure (GPa)
Open symbols: heating
Solid symbols: dcooling
(b)
0
100
200
300
400
500
600
700
Temperature (°C)

Fig.3

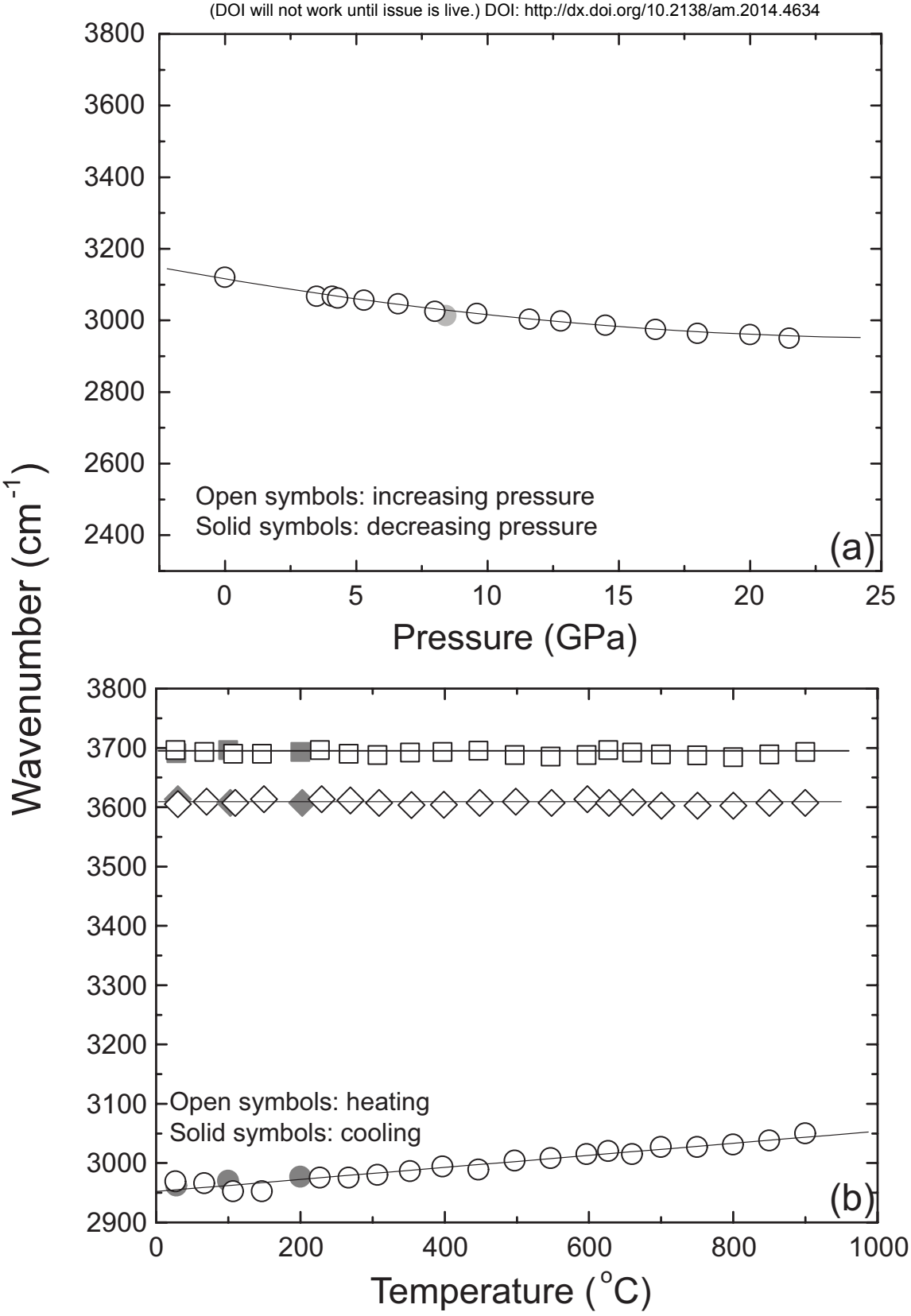
Wavenumber (cm-1)
Pressure (GPa)
Open symbols: increasing pressure
Solid symbols: decreasing pressure
(a)
Temperature (°C)
Open symbols: heating
Solid symbols: cooling
(b)

Fig. 4

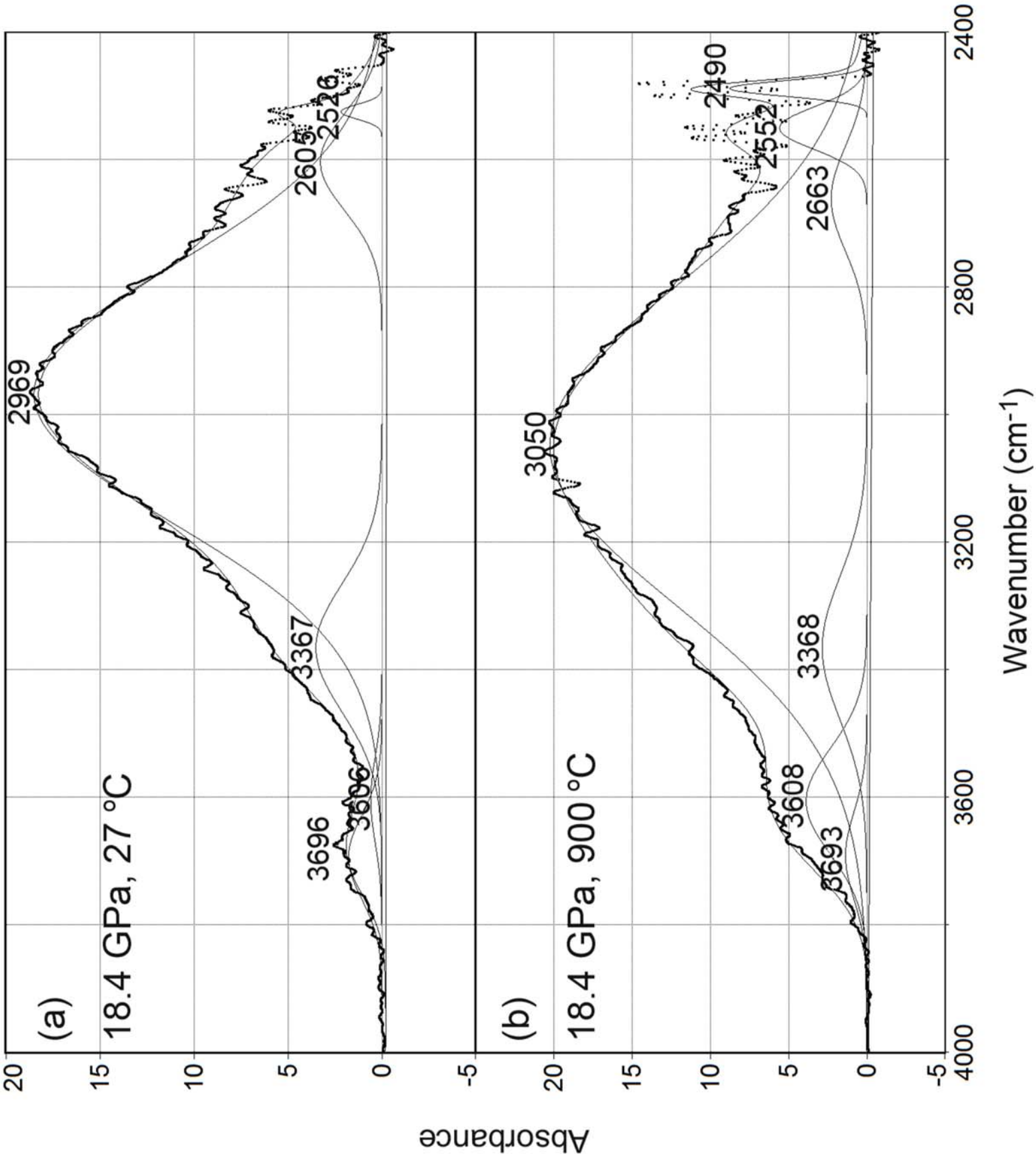
(a)
18.4 GPa, 27 °C
2969
2605
2526
3367
3696
3606
(b)
18.4 GPa, 900 °C
3050
2490
2552
2663
3368
3608
3693
Absorbance
Wavenumber (cm-1)
20
15
10
5
0
-5
2400
2800
3200
3600
4000

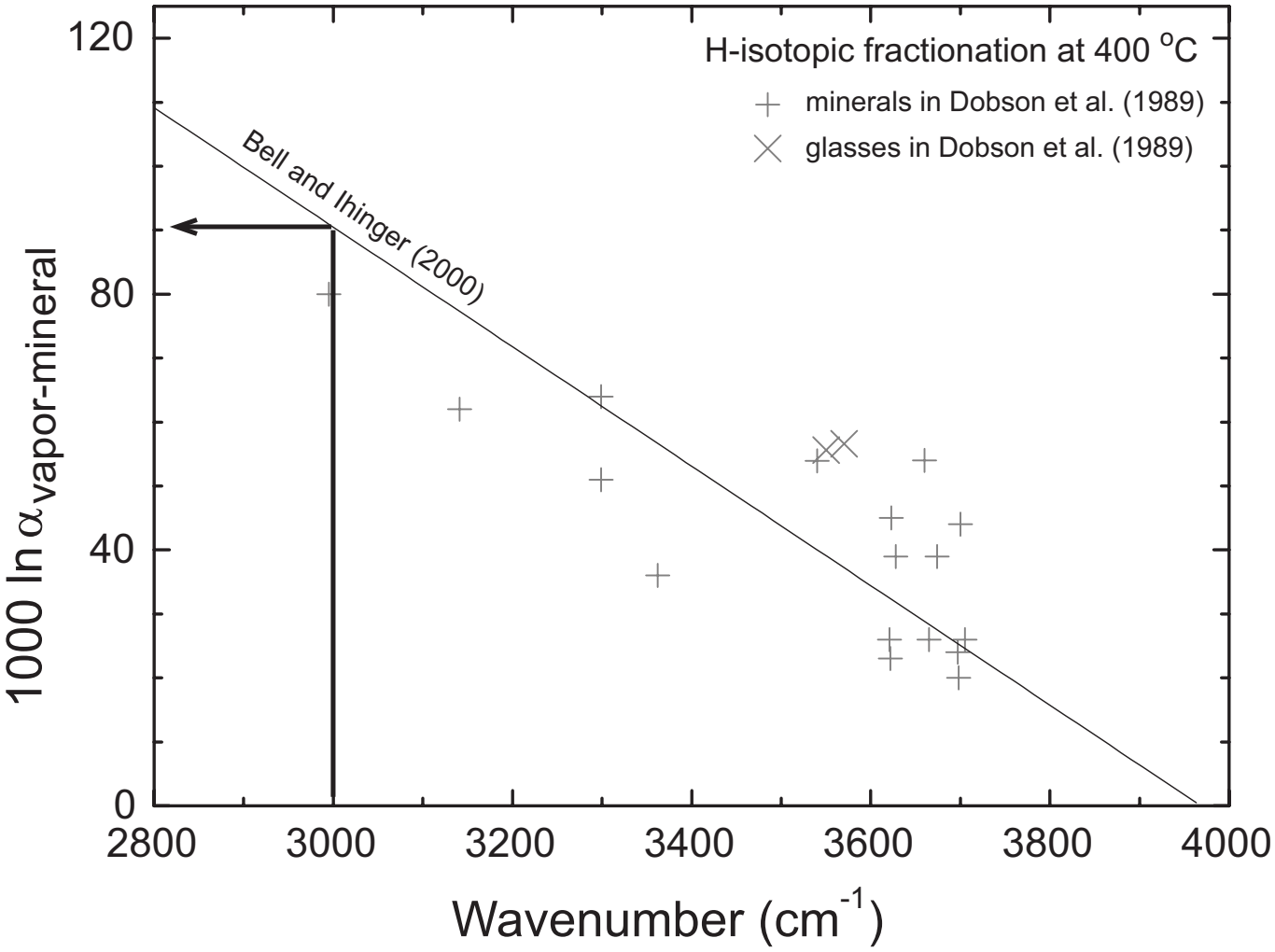
H-isotopic fractionation at 400 °C
minerals in Dobson et al. (1989)
glasses in Dobson et al. (1989)
Bell and Ihinger (2000)
1000 ln αvapor-mineral
Wavenumber (cm-1)
120
80
40
0
2800
3000
3200
3400
3600
3800
4000

Fig. 6